Theory of Methane Dehydrogenation on Pt{110}(1 × 2). Part I: Chemisorption of CH_x ($x = 0$ −3)

Melissa A. Petersen, Stephen J. Jenkins, and David A. King*

Department of Chemistry, University of Cambridge, Lensfield Road, Cambridge CB2 1EW, United Kingdom

Received: December 16, 2003

The chemisorption of methane dissociation intermediates, CH_x ($x = 0-3$), on Pt{110}(1 × 2) has been investigated using calculations based on density functional theory. For all species considered, the most stable adsorption site identified on the missing-row reconstructed (1 × 2) surface is the site that not only completes the tetravalency of the carbon atom but also involves the maximum number of ridge Pt atoms for a site of that type. Thus, methyl (CH_3) preferentially occupies the ridge atop site; methylene (CH_2), the ridge bridge site; methylidyne (CH), the fcc 3-fold site on the {111} microfacet; and carbon, the pseudosubsurface 4-fold site at the bottom of the trough. A comparison of the relative stability of the chemisorbed CH_x ($x = 0-3$) species reveals that CH is the most stable dissociation intermediate on Pt{110}(1 × 2).

I. Introduction

The interaction of hydrocarbon fragments with transition-metal surfaces has been the subject of extensive experimental and theoretical investigation.[1,2] The primary interest in such fragments stems from their involvement in hydrocarbon rearrangement and conversion reactions catalyzed by transition metals.[2,3] In particular, C_1 hydrocarbon fragments have been proposed as intermediates in such industrially relevant processes as the Fischer−Tropsch synthesis reaction,[2−7] catalytic steam reforming,[8,9,10] and methane partial oxidation.[11] To understand these reactions on a fundamental level with the aim of controlling and optimizing the processes, a knowledge of the elementary reaction steps and the intermediates involved is both necessary and desirable.

The dissociative chemisorption and subsequent decomposition of methane on the reconstructed Pt{110}(1 × 2) surface has been studied extensively using molecular beam techniques,[12−16] with a view toward elucidating the mechanism of methane partial oxidation on this surface.[17−21] In particular, Watson and co-workers[12,13] were able to identify the products of methane dissociative chemisorption on this surface as a function of surface temperature. In a series of experiments based on temperature-programmed reaction spectroscopy (TPRS), Watson et al.[12,13] established that methylidyne (CH) is the stable dissociation product at all coverages in the surface temperature range of 300−450 K and that at temperatures above 470 K methylidyne decomposes to adsorbed carbon and gaseous H_2. In addition, they found that at a saturation coverage of 0.25 ML methylidyne forms a c(2 × 4) ordered overlayer, as observed by LEED.[12,13,22] On the basis of the TPRS results, Watson[12] determined an activation energy of 121 ± 3 kJ mol^{-1} for methylidyne dehydrogenation to adsorbed carbon.

An investigation of the coverage dependence of the methane dissociative sticking probability[14] has revealed that methylidyne acts as a more efficient site blocker for methane dissociative adsorption than does carbon. Watson and co-workers suggested that this effect may be due to a difference in adsorption sites for the two decomposition fragments, coupled with a (1 × 2) → (1 × 1) structural transformation induced by the accumulation of carbon on the surface. Hydrogen−deuterium exchange experiments[23] further established that chemisorbed methylidyne can be deuterated to yield gaseous methane, whereas carbon formed as a result of methylidyne decomposition was stable to rehydrogenation over the surface temperature range of 250−700 K. The results were found to be consistent with a stepwise rehydrogenation mechanism, with more than 95% of the surface methylidyne being removed by deuteration.

Methyl (CH_3) fragments have been successfully prepared on Pt{111} using a variety of techniques, including the thermal[24−27] or photochemical[28,29] decomposition of adsorbed methyl halides, a methyl radical source generated from the pyrolysis of azomethane,[30,31] or the dissociative chemisorption of methane on the surface.[32] Oakes et al.[32] demonstrated that the primary product of methane dissociative adsorption on Pt{111} is a methyl moiety and concluded from their reflection−absorption infrared spectroscopy (RAIRS) analysis that the species is adsorbed with the 3-fold axis oriented perpendicular to the surface plane. Zaera[25−27] was further able to isolate both methyl and methylene fragments on Pt{111}, which were characterized using RAIRS, and argued that methylidyne fragments could be formed as well. Adsorbed methyl species have been observed to be thermally activated above ∼240 K on Pt{111},[25−27,29−32] resulting in the desorption of methane or the formation of dehydrogenation products. Fairbrother et al.[30,31] have demonstrated that the nature of the dehydrogenation products formed is dependent on the surface methyl and hydrogen coverage, with high methyl coverages favoring carbon coupling reactions and low methyl coverages ultimately resulting in thermal decomposition to adsorbed carbon. Although these studies relate to the chemisorption of CH_x ($x = 1-3$) fragments on Pt{111}, such studies indicate that the decomposition of methane on Pt{110}(1 × 2) may reasonably be expected to proceed through a set of sequential dehydrogenation steps, giving rise to adsorbed methyl, methylene, methylidyne, and ultimately carbon on the surface. Furthermore, the {111} facets on the reconstructed Pt{110}(1 × 2) surface are structurally similar to the Pt{111} surface.

A substantial number of theoretical studies of the adsorption of CH_x ($x = 1-3$) fragments on transition-metal surfaces and

* Corresponding author. E-mail: dak10@cam.ac.uk.

10.1021/jp037880z CCC: $27.50
Published on Web 04/15/2004

clusters now exist in the literature. The primary aim of such studies has been to determine the relative stability of adsorption sites for each fragment on the surface as well as the adsorption energetics, geometry, and electronic structure of the adsorbed species. Of additional interest is the origin of the site preference and reactivity for different metals. To this end, independent studies of the adsorption of CH_x ($x = 1-3$) fragments on Pt{111},[33-37] Ni{111},[38-48] Ru{0001},[49,50] Ru{1120},[51] Pd{111},[52,53] Pd{100},[54] Co{0001},[38,39,45,55] and Rh{111}[44] have been conducted. Comparative studies have been carried out by Zheng et al.[55] on Ti, Cr, and Co; Au et al.[56,57] on Ni, Pd, Pt, Cu, Ir, Os, Ru, Rh, Ag, and Au; and Goddard et al.[58] on Pt, Ir, Os, Pd, Rh, and Ru. The set of studies cited here is by no means exhaustive but serves to illustrate the extent of the current database for CH_x ($x = 1-3$) fragment adsorption on predominantly close-packed metal surfaces and representative clusters.

An intuitively appealing idea is that the CH_x fragment preferentially occupies a site that completes the carbon tetravalency such that CH_3 adsorbs at an atop site; CH_2, on a bridge site; and CH, in a 3-fold hollow site.[36,55] However, theoretical calculations have suggested that this rule may be violated for certain metals, with results on Ru{0001},[49,50,59] Cu{111},[56,57,60] and Ni{111}[40,42,43,46,47] indicating that CH_3 binds preferentially at a 3-fold hollow site instead of an atop site on these surfaces. High-resolution electron energy loss spectroscopy (HREELS) results for CH_3 adsorption on Ni{111}[61] are in support of the assignment of CH_3 to a 3-fold hollow site. Nevertheless, contradictory results do exist for Ni{111}, with some theoretical studies favoring the atop site for methyl chemisorption.[44,45] A similar preference for adsorption at the 3-fold site has been observed for methylene on Ni{111}[46,43,48] and Ru{0001}.[49] De Koster and van Santen[44] examined the effect of the valence electron occupation and the spatial extent of the d orbitals on the site preference for CH_x ($x = 1-3$) adsorption on Ni{111} within their parametrized atom superposition and electron delocalization (ASED) method. Interestingly, they observed a shift to higher coordination sites on decreasing either of these properties. Theoretical studies of CH_x ($x = 1-3$) adsorption on Pt{111} appear consistently to favor adsorption at sites that complete the carbon tetravalency of the CH_x species.[33-37]

The relative stability of adsorbed CH_x ($x = 0-3$) fragments has been determined in a number of theoretical studies. Goddard et al.[33,58] found that CH is the thermodynamic sink on clusters representing the close-packed surfaces of Pt, Ir, Os, Pd, Rh, and Ru. These results have been corroborated for Ru{0001},[49,50] Pt{111},[62] and Ni{111}[46] using periodic slab calculations, although Paul and Sautet[52] found that CH_3 is the most stable species on Pd{111}. More recent calculations have indicated that carbon is the most stable species on Pd{100},[54] whereas methylene is favored on Ru{1120}.[51]

In this paper, we present the results of extensive calculations of CH_x ($x = 0-3$) chemisorption on the missing-row reconstructed Pt{110}(1 × 2) surface. We treat each adsorbate in turn, identifying the lowest-energy adsorption site for each species, and provide a detailed analysis of the electronic structure of the stable intermediate adsorbed in the lowest-energy site in each case. We conclude with a comparison of the calculated relative stability of methane dissociation intermediates adsorbed on Pt{110}(1 × 2).

II. Calculation Methodology

Total-energy pseudopotential calculations were performed within the framework of density functional theory (DFT), as implemented in the CASTEP code.[63] The electronic wave functions were expanded in terms of a basis set of plane waves up to a kinetic energy cutoff of 310 eV. The exchange−correlation energy was described using the Perdew−Wang (PW91) form[64] of the generalized gradient approximation (GGA). Electron−ion interactions were described by ultrasoft pseudopotentials[65] on Pt, C, and H. A total of 10, 1, and 4 valence electrons for each Pt, H, and C atom, respectively, were thus explicitly treated in the calculations.

The calculations were performed using a supercell of length equivalent to 14 layers of Pt in the surface normal direction. The Pt{110} surface was represented by a six-layer slab within a (2 × 2) surface unit cell. The vacuum region between the slabs was thus equivalent to eight layers of Pt, ∼11 Å, thereby minimizing spurious interactions between neighboring slabs. The dimensions of the supercell were chosen to be consistent with the calculated conventional lattice parameter of 3.97 Å obtained using the GGA (experimental value 3.9236 Å[66]). This gave a supercell of dimensions 5.62 × 7.95 × 19.66 Å^3. Brillouin-zone integration was achieved by summation over a 4 × 3 × 1 Monkhorst−Pack mesh[67] of special **k** points. A Fermi-surface smearing of 0.2 eV was employed in the calculations, and the results were extrapolated to 0 K using the method of Gillan and de Vita.[68,69] Convergence with respect to the kinetic energy cutoff and the density of **k**-point sampling of the Brillouin zone was tested and found to be satisfactory. Spin polarization was not used in the calculations, except in the determination of the energetic and structural parameters of the isolated CH_x ($x = 0-3$) radicals.

The adsorbate was placed on one side of the slab, and both the adsorbate and the top four layers of the substrate were relaxed under the influence of the calculated forces. One adsorbate was placed in the (2 × 2) surface unit cell, resulting in a coverage of 0.25 ML (relative to the surface-layer atom density of the unreconstructed surface).

Atom-resolved charges have been obtained using the Bader topological method[70,71] in which the valence electron density is partitioned into regions attributable to each atom on the basis of topological features of the density distribution. This technique has been shown to be reliable and informative in a number of previous studies.[72-77]

III. Results and Discussion

The clean Pt{110}(1 × 2) surface exhibits a reconstruction of the missing-row form in which every alternate close-packed row aligned along the [1$\bar{1}$0] direction is absent.[78-81] The reconstruction leads to a highly corrugated surface consisting of a series of alternating ridges and troughs. The troughs, formed by the missing rows, are bound on either side by {111} microfacets. The sites considered for the adsorption of each of the CH_x ($x = 0-3$) fragments on Pt{110}(1 × 2) are illustrated schematically in Figure 1.

A. Methyl (CH_3) Adsorption on Pt{110}(1 × 2). *1. Adsorption Energetics and Site Preference.* Methyl adsorption was investigated at each of the sites shown in Figure 1, with the CH_3 species placed in two orientations at each site. Adsorption at three atop sites was thus considered, situated on the ridge (B), second (F), and third layers (K), for which one C−H bond of the CH_3 species was oriented either in the [1$\bar{1}$0] or the [001] direction in each case. In addition, one long-bridge (J) and four short-bridge (A, E, G, I) sites were investigated, at which one C−H bond was aligned either in the [001] or the [1$\bar{1}$0] direction for sites J, A, and G or in the direction of either of the two inequivalent bridge Pt atoms for sites E and I. Finally, three 3-fold sites (C, D, and H) were investigated, for which

TABLE 1: Selected Structural Parameters and Chemisorption Energy, E_{ads}, for CH_3 Adsorbed on the Pt{110}(1 × 2) Surface at a Coverage of 0.25 ML[a]

site	(orient.)	E_{ads} (eV)	d_{C-Pt} (Å)	d_{C-H} (Å)	d_{H-Pt} (Å)	∠HCH (deg)
B	**[1$\bar{1}$0], [001]**	**2.33**	**2.05 (1)**	**1.09 (3)**	**2.61 (2), 2.59 (1)**	**111 (3)**
A	[1$\bar{1}$0]	2.15	2.07 (1), 2.36 (1)	1.09 (2), 1.17 (1)	2.58 (2), 1.87 (1)	102 (2), 114 (1)
F	[1$\bar{1}$0], [001]	2.14	2.05 (1)	1.09 (3)	2.61 (2), 2.58 (1)	111 (3)
A	[001]	2.07	2.19 (2)	1.09 (1), 1.11 (2)	2.76 (1), 2.18 (2)	112 (2), 102 (1)
D	eclipsed	1.61	2.29 (2), 2.42 (1)	1.10 (1), 1.11 (2)	2.24 (1), 2.15 (2)	107 (3)
G	[001]	1.40	2.29 (2)	1.08 (1), 1.10 (2)	2.79 (1), 2.29 (2)	112 (2), 103 (1)
K	[1$\bar{1}$0]	1.22	2.03 (1)	1.09 (3)	2.58 (1), 2.57 (2)	112 (3)
J	[1$\bar{1}$0]	1.12	2.24 (2)	1.08 (1), 1.12 (2)	2.77 (1), 2.07 (2)	113 (2), 96 (1)
K	[001]	1.00	2.04 (1)	1.09 (3)	2.58 (3)	112 (3)

[a] Sites are labelled (orient.) according to whether one C−H bond is aligned along the [1$\bar{1}$0] or the [001] direction. Numbers in parentheses represent the number of bonds with that length. Where distinct, the shortest H−Pt distances are reported in the same order as the C−H lengths.

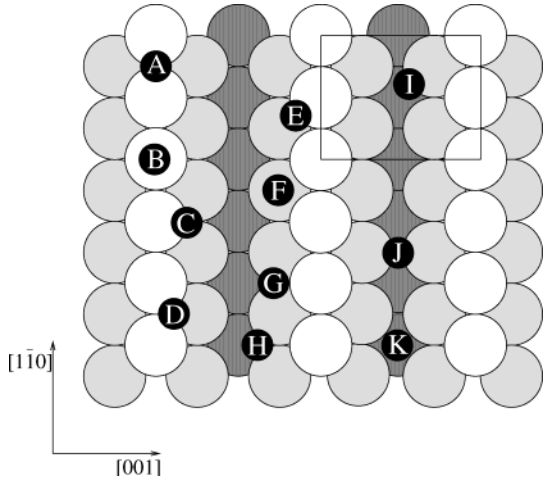

Figure 1. High-symmetry adsorption sites on Pt{110}(1 × 2). The (2 × 2) surface unit cell is indicated in the top right corner. White, light, and dark gray circles represent first-, second-, and third-layer Pt atoms, respectively, and black circles label adsorption sites.

the chosen alignment was either with the hydrogen atoms of the methyl group pointing toward the neighboring atop (eclipsed) or the bridge (staggered) positions of the 3-fold site. An energetic preference for the eclipsed geometry has, for example, been observed by Papoian et al.[34] in their calculations of CH_3 adsorption in the fcc 3-fold site on Pt{111}.

Not all of the sites that were initially considered were found to correspond to a stable adsorption geometry, with the methyl species moving instead into a neighboring site in some cases. For those sites that did result in a stable adsorption configuration, the corresponding optimized geometry and chemisorption energy, calculated with reference to the clean, relaxed Pt{110}-(1 × 2) surface and the isolated methyl radical in the singlet state, are summarized in Table 1.

The most stable site for methyl adsorption on Pt{110}(1 × 2) is the atop site located on the Pt ridge, site B. The corresponding calculated chemisorption energy for this site is 2.33 eV relative to the energy of the free CH_3 radical and the clean, relaxed surface. The calculated adsorption energy is similar to that obtained in previous theoretical studies of methyl adsorption on Pt{111}. Goddard et al.[33,58] obtained a binding energy of 2.33 eV for CH_3 adsorption in the atop site on Pt-{111} from their DFT cluster calculations, and Michaelides and Hu[37,60] determined a value of 2.05 eV from their DFT periodic slab calculations. A lower value of 1.77 eV was obtained by Au et al.[56,57] using the cluster approach, and Minot et al.[36] determined a similar adsorption energy of 1.74 eV within the framework of extended Hückel theory. A preference for CH_3 adsorption in the atop site on Pt{111} has been found in a number of theoretical studies.[33−37,56−58,60]

The stability of CH_3 adsorbed in the ridge atop site on Pt{110}(1 × 2) was found to be insensitive to rotation about the local molecular 3-fold axis, with the alignment of one C−H bond parallel to either the [1$\bar{1}$0] direction or the [001] direction, resulting in indistinguishable adsorption energies. A similar insensitivity to rotation was also observed for adsorption in the second-layer atop site (site F). In the latter case, the C−Pt bond axis was inclined at an angle of ∼5° with respect to the microscopic surface normal of the {111} microfacet in the optimized structure. A negligible barrier to rotation was similarly obtained by Zheng et al.[55] in their extended Hückel calculations of methyl adsorption in the atop site on the close-packed surfaces of Ti, Cr, and Co.

Adsorption in the remaining atop site located over a third-layer Pt at the bottom of the trough, site K, resulted in a considerably less stable configuration. As a consequence of adsorption, the Pt atom located directly below the methyl carbon is raised by 2.16 Å relative to the neighboring trough atoms. The vertical displacement of the substrate atom results in a stabilization of at least 0.32 eV; nevertheless, the trough atop site remains more than 1 eV higher in energy than the most stable adsorption site on the ridge. In addition, the stability of CH_3 adsorbed in the trough atop site (K) was found to be sensitive to the orientation of the fragment, with the C−H alignment along the [1$\bar{1}$0] direction being favored by 0.22 eV relative to the [001] alignment.

Of the three 3-fold sites (C, D, and H) initially investigated, only the fcc site (D) yielded a stable adsorption configuration. In this case, the optimized structure adopted the eclipsed geometry, with the hydrogen atoms directed toward the neighboring atop positions. For the staggered configuration, the CH_3 fragment drifted into the neighboring bridge site located on the close-packed ridge. Finally, CH_3 adsorption in the ridge bridge site (A) shows an energetic preference for the alignment of one of the C−H bonds along the close-packed Pt ridge, resulting in a tilted and distorted optimized adsorption geometry.

2. Stable Adsorption Geometry. A schematic illustration of CH_3 adsorbed in the most stable atop site on the ridge atoms of the Pt{110}(1 × 2) surface is shown in Figure 2. In the optimized structure, the C−Pt bond distance is 2.05 Å, and the C−H bonds are lengthened from 1.08 Å calculated for the isolated planar radical to 1.09 Å for the chemisorbed species. On adsorption, the hydrogen atoms of the methyl group are raised relative to the carbon atom so that the C−H bonds make an angle of ∼17° with respect to the horizontal. The structure of the adsorbate thus more closely approximates that of CH_4. The H−C−H angles are reduced from 120°, as calculated for the isolated planar radical, to 111° for chemisorbed CH_3. The corresponding Pt−C−H angles are 108° for the symmetrically equivalent H atoms and 107° for the remaining hydrogen atom.

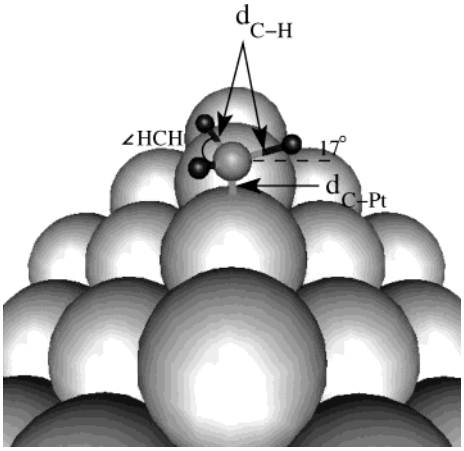

Figure 2. Schematic illustration of methyl (CH_3) chemisorbed in the most stable atop site on the close-packed ridge of the Pt{110}(1 × 2) surface. Large and small gray spheres represent Pt and carbon atoms, respectively, and H atoms are indicated in black.

The ridge atom coordinated to the methyl carbon is raised by 0.13 Å relative to the neighboring ridge atom.

Of additional interest is the optimized structure of CH_3 adsorbed in the ridge bridge site, with one C−H bond aligned along the close-packed row (site A). As indicated in Table 1, this adsorption configuration is characterized by one short C−Pt bond of 2.07 Å, similar to that obtained for the ridge atop site, and one long C−Pt bond of 2.36 Å. The CH_3 species is tilted in the [1$\bar{1}$0] direction so that the H atom aligned parallel to the Pt−Pt bond is brought closer to the surface. In the optimized structure, the corresponding C−H bond is lengthened to 1.17 Å, and the H−Pt distance is reduced to 1.87 Å. A similar tilted structure was obtained by Papoian et al.[34] for CH_3 adsorption in the bridge site on Pt{111}, and a related structure was determined by Michaelides and Hu[47] in their calculations of CH_3 adsorption in the bridge site on Ni{111}. In both cases, the tilted structure has been rationalized on the basis of agostic[82] interactions between the methyl hydrogen and the metal surface. Indeed, a correlation between the C−H bond length and the corresponding H−Pt distance is apparent in Table 1, with shorter H−Pt distances being coincident with a lengthening of the corresponding C−H bond.

3. Bonding Analysis of CH_3. The valence molecular orbitals of the isolated planar methyl radical are shown in Figure 3a. The lowest-energy $2a_1'$ orbital and the degenerate $1e'$ orbitals are fully occupied in the ground state, and the highest occupied $1a_2''$ orbital is partially occupied in the neutral radical. On adsorption of methyl in the atop site, these valence states may be expected to mix with metal states of appropriate symmetry and energy, resulting in the formation of the adsorbate−substrate bond.

The density of states (DOS) of the clean Pt{110}(1 × 2) surface projected onto the valence d states of a ridge Pt atom is shown in Figure 3b in combination with the discrete energy levels of the CH_3 molecular orbitals. On adsorption of CH_3 in the atop site, new peaks appear in the DOS, which may be more readily interpreted by considering the projection onto the carbon p and hydrogen s orbitals of methyl, shown in Figure 3c. The lowest-energy narrow peak at ∼11.9 eV below the Fermi level (E_f) in Figure 3c may be identified with a weak covalent interaction between the $2a_1'$ orbital and predominantly metal d states. Energy levels of the free radical (Figure 3a and b) have been aligned so that the $2a_1'$ orbital is level with this peak. The appearance of antibonding states of similar orbital character on the adsorbate near the bottom of the d band (at about −8.8 eV)

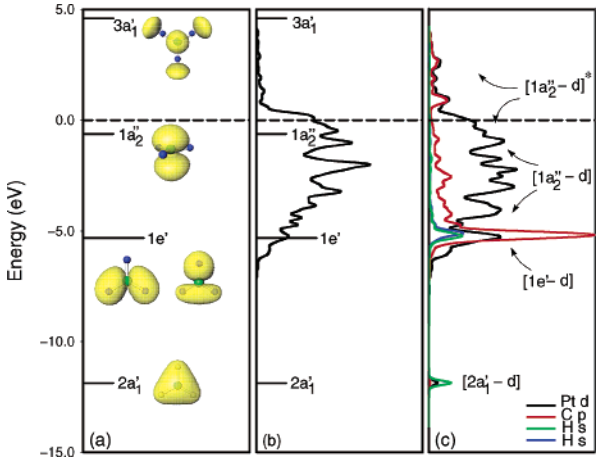

Figure 3. (a) Isosurfaces of the electron density distribution of the CH_3 valence orbitals. (b) Discrete energy levels of the isolated CH_3 radical and density of states (DOS) of the clean surface projected onto the valence d states of the ridge Pt atom of the atop site. (c) DOS of the chemisorption system projected onto the C p states (red), H s states (green, blue), and valence d states (black) of the same Pt atom as in plot b. The DOS has been referenced to the Fermi energy (E_f = 0).

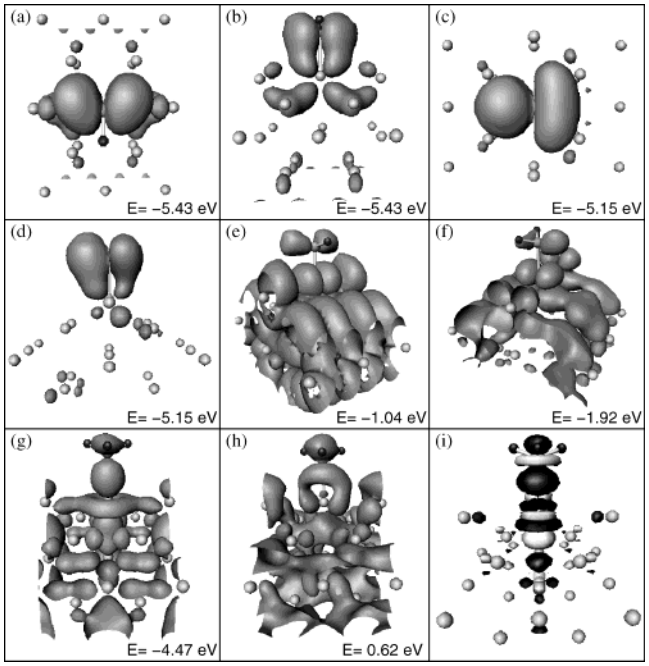

Figure 4. (a−h) Isosurfaces of the electron density distribution of individual eigenstates of the chemisorption system evaluated at $\bar{\Gamma}$. The isosurfaces correspond to electron densities of (a−d) 6.8 × 10^{-3}, (e) 1.6 × 10^{-4}, (f) 2.4 × 10^{-3}, (g) 3.4 × 10^{-3}, and (h) 2.4 × 10^{-3} electrons/Å^3. (i) Isosurfaces of the difference electron density. Dark-gray contours indicate an increase in density of 2.3 × 10^{-2} electrons/Å^3, and light-gray contours, a decrease in density by the same amount. Small gray spheres indicate Pt atoms, and small black spheres, the hydrogen atoms of the methyl group.

indicates that the interaction with the $2a_1'$ orbital results in a negligible contribution to the formation of the adsorbate−metal bond.

The largest carbon p peak ∼5.1 eV below the Fermi energy in Figure 3c may be attributed to states of predominantly $1e'$ orbital character. Two states of this type, obtained at $\bar{\Gamma}$, are shown in Figure 4a−d. The top views of the two eigenstates shown in Figure 4a and c display unmistakable $1e'$ orbital character on the adsorbate (compare with Figure 3a), and the corresponding rotated side views shown in Figure 4b and d demonstrate the mixing with metal states of d_{xz} and d_{yz} character

TABLE 2: Selected Structural Parameters and Chemisorption Energy, E_{ads}, for CH_2 Adsorbed on the Pt{110}(1 × 2) Surface at a Coverage of 0.25 ML[a]

site	(orient.)	E_{ads} (eV)	d_{C-Pt} (Å)	d_{C-H} (Å)	d_{H-Pt} (Å)	∠HCH (deg)
A	**(tetra)**	**4.61**	**2.03 (2)**	**1.09**	**2.65**	**115**
J	(tetra)	4.29	2.05 (2)	1.09	2.60	114
E	(tetra)	4.19	2.04 (1), 2.05 (1)	1.09	2.63, 2.68	113
E′	(tetra)	4.11	2.03 (2)	1.18, 1.09	1.85, 2.66	100
G	(tetra)	4.10	2.04 (2)	1.09	2.65, 2.70	113
D	[1$\bar{1}$0]	3.91	2.03 (1), 2.19 (2)	1.11	2.28	105
C	[1$\bar{1}$0]	3.61	2.02 (1), 2.23 (2)	1.10	2.33	106
B	[1$\bar{1}$0]	3.58	1.87 (1)	1.09	2.61	117
I	(tetra)	3.56	2.00 (1), 2.08 (1)	1.09, 1.11	2.52, 2.21	111
I′	(tetra)	3.56	2.02 (1), 2.09 (1)	1.09, 1.11	2.64, 2.14	111
B	[001]	3.53	1.87 (1)	1.09	2.61	117
H	[1$\bar{1}$0]	3.35	2.04 (1), 2.16 (2)	1.11	2.26	98
A	(planar)	3.28	2.01 (2)	1.11	2.19	105
K	[1$\bar{1}$0]	3.08	2.02 (1), 2.53 (4)	1.10	2.42	112
K	[001]	2.25	2.00 (1), 2.52 (4)	1.12	2.24	106
J	(planar)	2.05	1.99 (2)	1.13	2.04	98

[a] Twofold sites are labelled according to whether the carbon atom is in a tetrahedral (tetra) or planar environment. Numbers in parentheses for d_{C-Pt} represent the number of C−Pt bonds with that length. Where the two C−H bonds are of different length, both lengths are given, and the corresponding shortest H−Pt distances are cited in the same order. Primed entries indicate adsorption in the same site but with a distinct structure.

localized on the atop Pt atom (*z* perpendicular to the surface). The 1e′ orbitals lie within the molecular plane of the isolated CH_3 fragment, which suggests that they may be subject to relatively poor orbital overlap with the metal states on the atop Pt atom as the adsorbate approaches the surface. Of greater significance is the fact that the out-of-phase combinations of the 1e′ orbitals with the metal states fall below the Fermi level, suggesting that the net covalent interaction of all of the 1e′ orbitals with the metal states is destabilizing. Representative antibonding eigenstates of 1e′ character obtained at $\bar{\Gamma}$ are shown in Figure 4e and f.

Mixed states exhibiting strong $1a_2''$ orbital character on the CH_3 fragment are distributed throughout the d band. The appearance of states of this type near the bottom of the d band with appreciable amplitude on the methyl fragment is indicative of a strong bonding interaction with the surface. A typical state of this type at $\bar{\Gamma}$ is shown in Figure 4g, in which the orbital overlap with a state of d_{z^2} character on the metal atop atom is clearly evident. This particular state bears a striking resemblance to the region of electron density increase indicated by the dark gray contours in the difference electron density distribution shown in Figure 4i. This difference distribution is evaluated by subtracting the sum of the total density of the isolated CH_3 fragment and the clean surface, each constrained in the adsorption configuration, from the total density of the chemisorption system. Corresponding adsorbate−metal antibonding mixed states may be found at higher energies both below and above the Fermi energy. A representative unoccupied antibonding state at $\bar{\Gamma}$, coinciding with the first carbon p peak ∼0.7 eV above the Fermi energy in Figure 3c, is shown in Figure 4h. The strong bonding interaction of the $1a_2''$ orbital with metal states, together with the appearance of corresponding unoccupied antibonding states above the Fermi energy, suggests that the $1a_2''$ state is the main contributor to the net stabilization of the covalent adsorbate−metal bond.

B. Methylene (CH_2) Adsorption on Pt{110}(1 × 2). *1. Adsorption Energetics and Site Preference.* The sites considered for methylene adsorption on Pt{110}(1 × 2) are shown in Figure 1. For the short (A, E, G, and I) and long (J) bridge sites, two orientations of the CH_2 species were considered, with the carbon atom located in either a planar or tetrahedral environment with respect to the relative orientation of the C−H and C−Pt bonds. For the remaining sites, the HCH plane was orientated in either the [1$\bar{1}$0] direction along the close-packed rows or in the [001] direction. As before, not all of the sites that were initially investigated were found to correspond to a critical point on the potential energy hypersurface. For those sites that did result in a stable adsorption geometry, the corresponding chemisorption energy and optimized structural parameters are summarized in Table 2.

The lowest-energy adsorption site is the short bridge site on the Pt ridge (site A), with the carbon atom in a tetrahedral environment. The corresponding chemisorption energy, calculated with reference to the clean, relaxed Pt{110}(1 × 2) surface and the isolated methylene radical in the triplet state, is 4.61 eV. A strong preference for the tetrahedral orientation over that of the planar arrangement is evident in Table 2, resulting, for example, in a binding energy difference of 1.33 eV for the two configurations at the ridge bridge site. A strong preference for adsorption in 2-fold sites as opposed to adsorption in higher- or lower-coordination sites is also evident, indicating that the carbon atom of the methylene species has a tendency to complete its tetravalency on binding to the Pt{110}(1 × 2) surface.

Although the binding energy of CH_2 on Pt{110}(1 × 2) has not been determined experimentally, previous theoretical calculations of CH_2 adsorption on Pt{111} have yielded similar chemisorption energies. For adsorption in the bridge site on Pt{111}, Michaelides and Hu[37] obtained a binding energy of 4.06 eV using DFT periodic slab calculations, and Goddard et al.[33,58] obtained a value of 4.52 eV using the cluster approach. An earlier extended Hückel calculation determined a lower binding energy of 3.90 eV.[36] In the present study on Pt{110}-(1 × 2), a chemisorption energy of 4.61 eV for adsorption in the ridge bridge site corresponds to an average C−Pt bond energy of 2.30 eV/bond. This is (fortuitously) identical to the average value for the C−Pt bond strength obtained by Kua and Goddard[33] from their cluster calculations of CH_x ($x = 1-3$) chemisorption on Pt{111}.

2. CH_2 Adsorption Geometry. The isolated methylene radical occurs in a lower-energy triplet state and a higher-energy singlet state.[84,85] The structural parameters were thus determined for both states. The calculated C−H bond length obtained for the triplet state is 1.08 Å, with a HCH bond angle of 138° (experimental values[66] 1.078 Å and 130°), and for the singlet state, the corresponding calculated values are 1.09 Å and 121°. The triplet state was found to be favored by 0.39 eV.

For CH_2 adsorbed in the ridge bridge site, the calculated

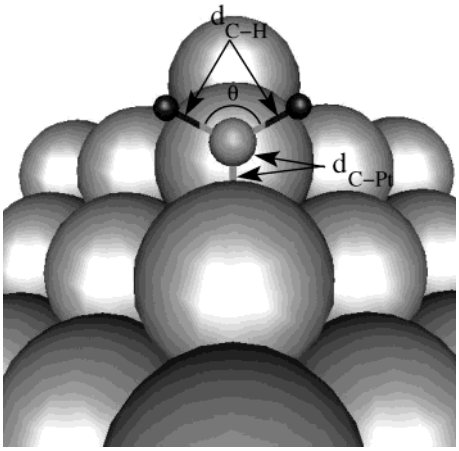

Figure 5. Schematic illustration of methylene (CH_2) chemisorbed with a tetrahedral orientation in the ridge bridge site on the Pt{110}(1 × 2) surface.

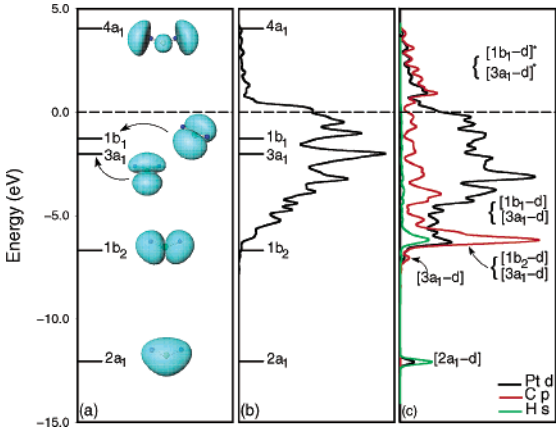

Figure 6. (a) Isosurfaces of the electron density distribution of the CH_2 valence orbitals. (b) Discrete energy levels of the isolated CH_2 radical and density of states (DOS) of the clean surface projected onto the valence d states of a ridge Pt atom. (c) DOS of the chemisorption system projected onto the C p states (red), H s state (green), and valence d states (black) of the same Pt atom as in plot b. The DOS has been referenced to the Fermi energy indicated by the dashed line ($E_f = 0$).

optimal C−Pt bond length is 2.03 Å, and the C−H bond is lengthened from 1.08 Å in gas-phase CH_2 in the triplet state to 1.09 Å on the surface. In addition, the HCH angle (θ in Figure 5) is reduced from 138° for the triplet radical to 115° for the chemisorbed fragment. The structural parameters of chemisorbed CH_2 thus more closely resemble those of the radical in the singlet state. This is consistent with a quenching of the residual spin of the triplet CH_2 species by the Pt valence electrons on adsorption of the radical on the surface.

The optimal adsorption configuration of CH_2 in the lowest-energy site is illustrated schematically in Figure 5. It is worth noting that the potential energy surface (PES) is relatively flat in the [001] direction in the region of the ridge bridge site. The CH_2 fragment may be displaced by as much as 0.14 Å away from the ideal bridge site in the [001] direction (i.e., across the ridge) without any significant change in energy being observed.

3. Bonding Analysis of CH_2. Isosurfaces of the electron density distribution of the valence orbitals of the free CH_2 radical are shown in Figure 6a. In the neutral species, the lowest-energy $2a_1$ and $1b_2$ states are both fully occupied. The remaining two valence electrons occupy the $3a_1$ orbital in the singlet state, and in the triplet state, both the $3a_1$ and the $1b_1$ orbitals are partially occupied.

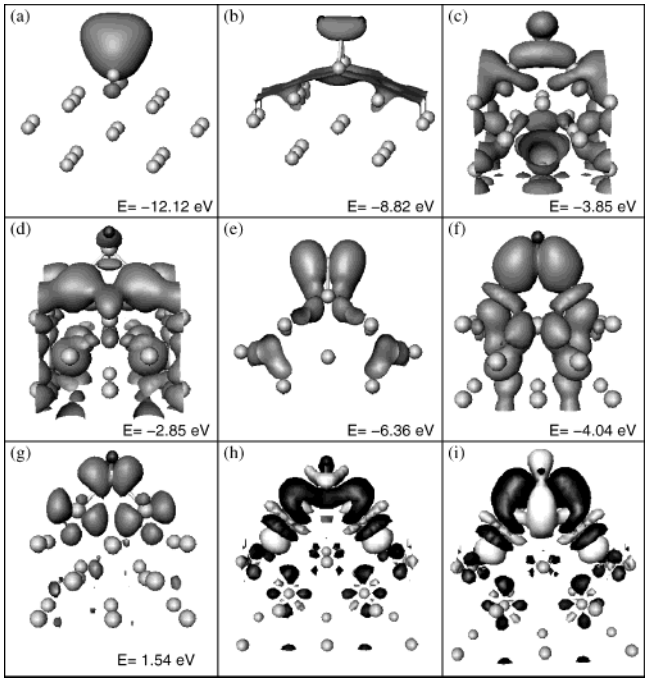

Figure 7. (a−g) Isosurfaces of the electron density distribution of individual eigenstates of the CH_2 chemisorption system evaluated at $\bar{\Gamma}$. The isosurfaces correspond to electron densities of (a) 6.8×10^{-3}, (b) 1.0×10^{-3}, (c) 3.7×10^{-3}, (d) 1.7×10^{-3}, (e) 6.8×10^{-3}, (f) 4.0×10^{-3}, and (g) 8.0×10^{-3} electrons/Å^3. (h, i) Isosurfaces of the difference electron density evaluated with CH_2 in the triplet (h) and singlet (i) states. Dark-gray contours indicate an increase in density of 2.3×10^{-2} electrons/Å^3, and light-gray contours, a decrease in density by the same amount. The angle of view in plots a, b, and e is down the close-packed ridge in the [110] direction; the remaining plots are viewed across the ridge in the [001] direction. In all cases, the Pt atoms are indicated by small, light-gray spheres.

The density of states of the chemisorption system projected onto the carbon p and hydrogen s orbitals and onto the valence d states of a ridge Pt atom is shown in Figure 6c. For comparison, the projection onto the d states of the same Pt atom on the clean surface is shown in Figure 6b, together with the discrete energy levels of the free CH_2 radical. In Figure 6a and b, the $2a_1$ level has been aligned with the lowest-energy peak in Figure 6c. This alignment of the CH_2 energy levels provides qualitative insight into the degree to which each orbital contributes to the formation of the covalent adsorbate−substrate bond.

The lowest-energy peak in Figure 6c (∼12.1 eV below E_f) corresponds to a weakly covalent interaction between the $2a_1$ orbital of the CH_2 species and the d states of the bridge Pt atoms. A representative eigenstate determined at $\bar{\Gamma}$ is shown in Figure 7a, in which the $2a_1$ orbital character is clearly evident on the CH_2 species (compare with Figure 6a). The corresponding antibonding combination appears near the bottom of the d band (∼8.8 eV below E_f at $\bar{\Gamma}$) and exhibits a weak amplitude on the adsorbate. The electron density distribution of such an antibonding state, determined at $\bar{\Gamma}$, is shown in Figure 7b.

The lowest-energy carbon p peak occurring ∼7.1 eV below the Fermi level originates from mixing between the $3a_1$ orbital and the metal d states. The appearance of states with significant $3a_1$ character on the CH_2 species that are shifted down in energy to the bottom of the d band is indicative of a strong interaction of this fragment orbital with the d states of the metal. Bonding interactions of this type are observed up to ∼2.9 eV below the Fermi level. An example of such a state is illustrated in Figure 7c, in which the overlap between the lower lobe of the $3a_1$ orbital

and states of d_{z^2} character on the ridge bridge Pt atoms is evident. At higher energies ($E > -2.9$ eV), antibonding combinations of the $3a_1$ fragment orbital with the metal valence states may be identified, a particularly clear example of which is shown in Figure 7d. Such antibonding interactions may be found both below and above the Fermi level in the chemisorption system. This is consistent with the region of electron density decrease of $3a_1$ character observed in the difference electron density distribution of Figure 7i, evaluated with reference to singlet CH_2 constrained in the adsorption geometry. The $3a_1$ orbital is fully occupied in singlet CH_2 so that a density decrease indicates a net depopulation of states of $3a_1$ character on adsorption. In Figure 7h and i, the density difference distribution has been determined by subtracting the sum of the total density of the triplet (Figure 7h) or singlet (Figure 7i) CH_2 radical and the clean surface, both constrained in the optimized adsorption configuration, from the total electron density of the chemisorption system in each case.

The largest carbon p peak in Figure 6c, about 6.2 eV below the Fermi energy, includes states that exhibit strong $1b_2$ character. The lowest-energy state of this type at $\bar{\Gamma}$, which exhibits clear mixing with the d states of the ridge atoms, is shown in Figure 7e. Additional states with $1b_2$ character are found at higher energies below the Fermi level, but such states do not appear to display any clear mixing with the metal orbitals at $\bar{\Gamma}$ and may be either nonbonding or antibonding in character. The presence of relatively few bonding combinations in the chemisorption system and the absence of adsorbate−metal antibonding states above the Fermi level indicate that the $1b_2$ orbital makes only a minor contribution to the stabilization of the CH_2−metal covalent bond.

The $1b_1$ orbital, which is the highest occupied orbital in the triplet CH_2 radical, is orientated along the close-packed ridge when CH_2 is adsorbed in the lowest-energy bridge site with the carbon atom in a tetrahedral environment. This enables the $1b_1$ orbital to interact strongly with the metal states, as shown for example in Figure 7f. The largest carbon p peak in Figure 6c, which appears near the bottom of the d band in the chemisorption system, includes states that display strong $1b_1$ orbital character on the CH_2 species. The corresponding antibonding orbitals are predominantly pushed above the Fermi level so that the $1b_1$ orbital provides a net stabilizing contribution to the chemisorption system. A typical unoccupied antibonding state is shown in Figure 7g. The region of electron density increase along the CH_2−metal bonds shown in Figure 7h and i exhibits strong $1b_1$ character, even in the case of the density difference distribution evaluated with respect to the triplet CH_2 radical (Figure 7h), in which the $1b_1$ orbital is already partially occupied.

The strong energetic preference for the tetrahedral orientation of the CH_2 fragment over the planar geometry may be attributed to the alignment of the $1b_1$ orbital along the close-packed Pt ridge in the former case. This alignment enables the $1b_1$ orbital to overlap effectively with the antibonding metal states near the top of the d band, resulting in a strong CH_2−metal bonding interaction. As the HCH plane is rotated into the planar configuration, the interaction of the $1b_1$ orbital with the metal states may be expected to decrease. In the planar geometry, the $1b_2$ orbital is now aligned along the close-packed ridge, but the large energy difference between this orbital and the antibonding metal states of appropriate symmetry near the top of the d band suggests that the resulting interaction will not be sufficient to compensate for the reduction in the contribution of the $1b_1$ orbital to the bonding as a result of CH_2 being rotated into the planar configuration.

TABLE 3: Selected Structural Parameters and Chemisorption Energy, E_{ads}, for CH Adsorption on the Pt{110}(1 × 2) Surface at a Coverage of 0.25 ML[a]

site	E_{ads} (eV)	d_{C-Pt} (Å)	d_{C-H} (Å)	tilt angle (deg)
D	**6.72**	**2.00 (3)**	**1.09**	**30.9**
C	6.61	1.99 (1), 2.00 (2)	1.09	30.6
H	6.39	1.97 (2), 2.02 (1)	1.09	35.9
A	6.25	1.90 (2)	1.09	0
I	6.16	1.99 (2), 2.08 (1)	1.09	34.7
J	5.97	2.05 (2), 2.06 (2)	1.10	0.7
K	5.36	2.04 (1), 2.29 (4)	1.09	0
B	4.44	1.77 (1)	1.09	0

[a] Numbers in parentheses for d_{C-Pt} represent the number of C−Pt bonds of that length. The CH tilt angle is relative to the macroscopic surface normal and is in the [001] direction, except for site I, for which the tilt is in the [1$\bar{1}$0] direction.

C. Methylidyne (CH) Adsorption on Pt{110}(1 × 2). *1. Adsorption Energetics and Site Preference.* As an extension of a previous study[22] in which CH adsorption on Pt{110}(1 × 2) was discussed in the context of the c(2 × 4) ordered overlayer structure observed experimentally by Watson and co-workers for this system,[12,13] we next consider CH chemisorption on this surface. The calculated chemisorption energies and structural parameters characterizing adsorption at each of the sites illustrated in Figure 1 are summarized in Table 3. Only those sites for which a stable adsorption configuration was obtained are included in Table 3. Methylidyne chemisorption preferentially occurs in the fcc 3-fold hollow site (site D) situated on the {111} microfacets that make up the trough walls on the reconstructed surface. The calculated binding energy of 6.72 eV obtained for adsorption in this site corresponds to an average C−Pt bond energy of 2.24 eV/bond. By comparison, an average C−Pt bond strength of 2.28 eV/bond was estimated for ethylidyne (CCH_3) chemisorbed on Pt{110}(1 × 2) using single-crystal adsorption calorimetry.[86] Thus, there is striking agreement between the calculated and measured values of the C−Pt bond strength for a carbyne chemisorbed in a 3-fold site on this surface.

Previous theoretical calculations of CH chemisorption on the Pt{111} surface have yielded similar chemisorption energies to that obtained in the current study on the Pt{110}(1 × 2) surface. Michaelides and Hu[37] determined a binding energy of 6.84 eV for CH adsorption in the fcc 3-fold site on Pt{111} in their DFT periodic slab calculations, and Au et al.[56,57] and Goddard et al.[33,58] obtained values of 6.71 and 7.23 eV, respectively, using the cluster approach. In an earlier extended Hückel cluster calculation,[36] a value of 6.73 eV was determined. In all cases, the 3-fold hollow site was found to be the most stable site for adsorption of methylidyne on the Pt{111} surface.

The next most stable site (Table 3), the hcp 3-fold site (C), is 0.11 eV less stable than the fcc site (D), and the "lower" fcc site (H) located at the bottom of the {111} facet is 0.33 eV less stable than the "upper" fcc site (D). The ridge bridge site (A) was found to be stable within the initial symmetry-constrained calculations, but upon further investigation with relaxed symmetry, this site was found to correspond to a saddle point on the potential energy surface and not a local minimum. Sites labeled E, F, and G in Figure 1 did not correspond to a critical point on the potential energy surface. A CH fragment placed in the bridge site (E) or atop site (F) moved instead into the most stable fcc 3-fold site (D), and CH placed in the bridge site (G) moved to the hcp 3-fold site (C). Finally, adsorption in site I resulted in a 3-fold-coordinated species, which is displaced from

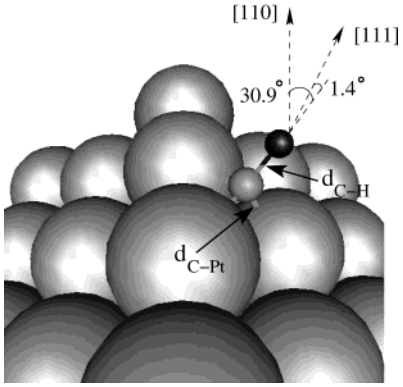

Figure 8. Schematic illustration of methylidyne (CH) chemisorbed in the most stable adsorption site on the Pt{110}(1 × 2) surface.

the long-bridge site (J) in the [1$\bar{1}$0] direction and is tilted by 34.7° relative to the macroscopic surface normal.

2. CH Adsorption Geometry. For CH chemisorbed in the most stable 3-fold site, the calculated optimal C−Pt bond length is 2.00 Å, and the C−H bond is contracted from 1.12 Å in the free radical (experimental bond length 1.1199 Å[66]) to 1.09 Å for the chemisorbed fragment. This latter value more closely approximates that in methane, for which the corresponding experimentally determined C−H bond length is 1.0870 Å[66] and the calculated value is 1.09 Å. On the surface, the CH fragment is tilted away from the Pt ridge in the [001] direction by 30.9° relative to the macroscopic surface normal. The C−H axis is thus oriented approximately perpendicular to the plane of the {111} fragment, deviating by 1.4° with respect to the microscopic surface normal. The optimal structure is illustrated schematically in Figure 8.

On adsorption of CH, the ridge Pt atoms are each displaced by 0.03 Å in the [1$\bar{1}$0] direction away from the adsorbate and are raised by 0.11 Å. Similarly, the second-layer Pt atom to which the CH fragment is bonded is displaced by 0.09 Å in the [001] direction away from the adsorbate and raised by 0.12 Å. The remaining substrate atoms undergo only minor displacements in response to the presence of the adsorbate, relative to their positions on the relaxed, clean surface.

3. Bonding Analysis of CH. Isosurfaces of the electron density distribution of the gas-phase CH fragment orbitals are shown in Figure 9a. The set of valence orbitals consists of doubly occupied 2σ and 3σ bonding C−H combinations and a pair of 1π orbitals that essentially correspond to the nonbonding carbon p_x and p_y orbitals, only one of which is occupied by a single electron. The unoccupied antibonding 4σ* and 5σ* orbitals lie above the 1π set.

The density of states of the chemisorption system, projected onto the carbon 2p orbitals and onto the hydrogen 1s orbital, is shown in Figure 9c in combination with the projection onto the valence d states of the second-layer Pt atom to which the methylidyne fragment is bonded. For comparison, the projection onto the d states of the same Pt atom on the clean surface is shown in Figure 9b in combination with the discrete energy levels of the isolated radical. In Figure 9a and b, the discrete levels have been aligned with the lowest-energy peak in Figure 9c.

The electron density distribution of the lowest-energy valence state at $\bar{\Gamma}$ in the chemisorption system, corresponding to the lowest-energy peak ~12.3 eV below E_f in Figure 9c, is shown in Figure 10a. A weak bonding interaction between the 2σ orbital and the metal states on the substrate atoms of the 3-fold site is evident. The bonding nature of this state is borne out by

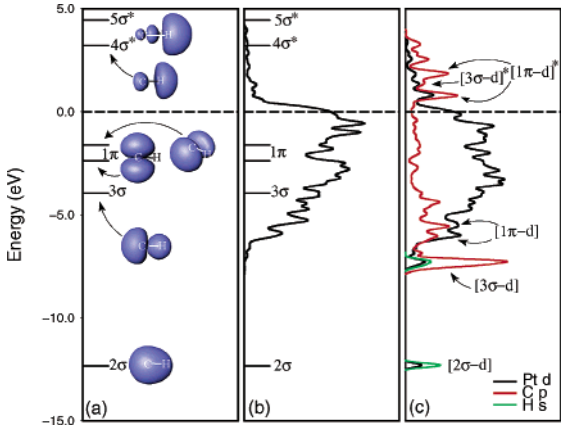

Figure 9. (a) Isosurfaces of the electron density distribution of the CH valence orbitals. (b) Discrete energy levels of the isolated CH radical and density of states (DOS) of the clean surface projected onto the valence d states of a single surface Pt atom. (c) DOS of the chemisorption system projected onto the C p states (red), H s state (green), and valence d states (black) of the same Pt atom as in plot b. The DOS has been referenced to the Fermi energy indicated by the dashed line ($E_f = 0$).

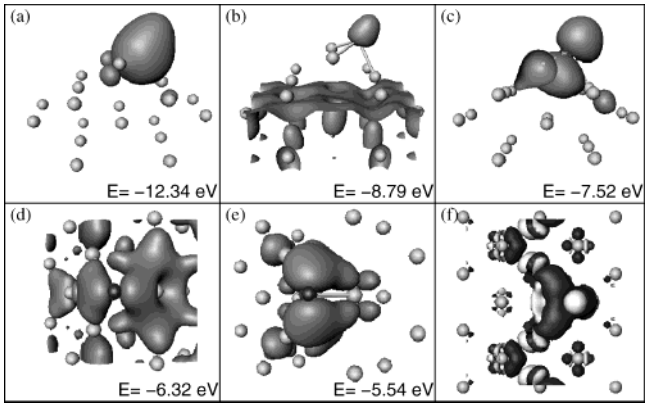

Figure 10. (a−e) Isosurfaces of the electron density distribution of individual eigenstates of the chemisorption system evaluated at $\bar{\Gamma}$. The isosurfaces correspond to electron densities of (a, c−e) 6.8 × 10^{-3} electrons/Å^3 and (b) 3.4 × 10^{-3} electrons/Å^3. (f) Isosurfaces of the difference electron density. Dark-gray contours indicate an increase in density of 2.3 × 10^{-2} electrons/Å^3, and light-gray contours, a decrease in density by the same amount. The angle of view is down the close-packed ridge in the [1$\bar{1}$0] direction in plots a−c, in the [111] direction normal to the microfacet in plots d and e, and in the [110] direction normal to the macroscopic surface plane in plot f.

the appearance of a second, antibonding state near the bottom of the d band. This state, illustrated in Figure 10b, exhibits appreciable density on the metal slab while retaining the orbital character of the 2σ state on the CH fragment. The presence of occupied bonding and antibonding combinations involving the 2σ orbital indicates that the mixing of this orbital with states on the substrate atoms results in a net destabilizing contribution to the formation of the covalent bond.

The largest carbon p peak in Figure 9c (~7.3 eV below E_f) corresponds to a bonding interaction between the 3σ orbital of the fragment and the d states of the metal. The lowest-energy state of this nature at $\bar{\Gamma}$ is shown in Figure 10c. The appearance of similar states above the Fermi level, but with antibonding character, is consistent with a loss of electron density from the 3σ state relative to that of the gas-phase radical. Isosurfaces of the difference electron density are shown in Figure 10f, in which regions of electron density increase (decrease) are indicated in dark (light) gray. The difference distribution is evaluated by subtracting the sum of the total density of the isolated CH

TABLE 4: Calculated Chemisorption Energies, E_{ads}, and Selected Structural Parameters Characterizing Atomic Carbon Adsorption on Pt{110}(1 × 2) at a Coverage of 0.25 ML[a]

site	E_{ads} (eV/C atom)	d_{C-Pt} (Å)
J	**7.19**	**1.93 (2), 2.02 (2)**
D	7.08	1.91 (2), 1.92 (1)
C	7.05	1.87 (1), 1.92 (2)
H	6.60	1.89 (2), 1.93 (1)
A	6.51	1.86 (2)
K	6.46	2.01 (1), 2.11 (4)
I	6.37	1.93 (1), 1.97 (1), 1.99 (1)
B	5.06	1.75 (1)

[a] Numbers in parentheses for d_{C-Pt} represent the number of C−Pt bonds of that length.

TABLE 5: Selected Structural Parameters and Chemisorption Energy, E_{ads}, for Atomic Hydrogen Adsorbed on the Pt{110}(1 × 2) Surface at a Coverage of 0.25 ML[a]

site	E_{ads} (eV/($^1/_2$)H_2)	d_{H-Pt} (Å)
A	**0.64**	**1.75 (2)**
D	0.58	1.86 (2), 1.87 (1)
E	0.55	1.75 (1), 1.80 (1)
F	0.55	1.56 (1)
B	0.53	1.57 (1)
C	0.49	1.87 (3)
H	0.40	1.82 (2), 1.91 (1)
J	0.30	1.84 (2)
K	0.05	1.60 (1)

[a] Numbers in parentheses for d_{H-Pt} represent the number of H−Pt bonds of that length.

fragment and the clean surface, both constrained in the adsorption configuration, from the total density of the chemisorption system. The region of electron density decrease on the CH fragment may reasonably be attributed to a loss of density predominantly from states arising from the 3σ orbital. This loss in 3σ density must outweigh any possible gain in 4σ* density due to mixing with metal states near the top of the d band.

The region above the principal [3σ−d] peak in Figure 9c from approximately −6.5 to −2.3 eV includes states that involve mixing between the 1π orbitals and the metal valence d states. Representative interactions are shown in Figure 10d and e in which the electron density isosurfaces are viewed down the axis of the CH fragment. A comparison of Figure 9b and c suggests that the 1π orbitals interact more strongly than the 3σ orbital with the metal states. The presence of unoccupied antibonding combinations of [1π−d] states in the energy region above the Fermi level is indicative of a net stabilizing interaction. The region of electron density increase aligned along the C−Pt bonds in Figure 10f may be associated predominantly with the increased population of the 1π states relative to that of the free radical.

D. Atomic Carbon Adsorption on Pt{110}(1 × 2). Selected structural parameters and chemisorption energies characterizing the adsorption of atomic carbon in each of the sites illustrated in Figure 1 are summarized in Table 4. As before, not all of the adsorption sites that were initially considered for carbon adsorption, and that are illustrated in Figure 1, were found to correspond to a local minimum on the PES. In particular, a carbon atom placed in the bridge site between the first and second Pt layers (site E) or in the atop position on the second layer (site F) moved into the neighboring fcc site on the side of the Pt ridge (site D). Similarly, a carbon atom placed in the second-layer bridge site (G) moved into the neighboring hcp site (C). Finally, carbon placed in the bridge site between the second and third layers on the {111} microfacet (site I) also moved into a 3-fold site similar to site H, but with a higher energy (by 0.23 eV) and slightly different geometry (Table 4). In all cases, therefore, the carbon atom is displaced to a neighboring site that offers the possibility of increased coordination of the adatom to the surface.

The most stable site for carbon adsorption on Pt{110}(1 × 2) is the 4-fold site in the trough (site J). In this site, the carbon adatom is located between the second and third layers at corresponding C−Pt distances of 1.93 and 2.02 Å, respectively. The carbon atom is located 0.16 Å below the second-layer Pt atoms to which it is coordinated, which are in turn raised 0.30 Å relative to the neighboring second-layer atoms in the (2 × 2) surface unit cell. The buckling of 0.28 Å exhibited in the third substrate layer on the clean surface[81] is reduced to 0.13 Å in the presence of atomic carbon as the third-layer substrate atoms to which the adsorbate is bonded move down to accommodate the carbon atom.

The chemisorption energy for atomic carbon adsorbed in the lowest-energy trough site on the (1 × 2) surface is 7.19 eV/C atom relative to the clean, relaxed surface and an isolated C atom. Comparative values obtained for adsorption in the most stable 3-fold hollow site on the Pt{111} surface are 6.60 eV/C atom[33] and 7.40 eV/C atom[56,57] obtained using the cluster approach and 6.86 eV/C atom based on periodic slab calculations.[37]

E. Hydrogen Adsorption on Pt{110}(1 × 2). To determine the relative stability of the chemisorbed CH_x ($x = 0-3$) intermediates in the presence of coadsorbed atomic hydrogen, we investigated the adsorption of hydrogen adatoms on Pt{110}-(1 × 2) at a coverage of 0.25 ML. The chemisorption energy and optimized adsorption geometry for each of the sites explored in Figure 1 are summarized in Table 5, in which the chemisorption energy per H atom is referenced to half the energy of an isolated hydrogen molecule in the gas phase at "infinite" separation from the clean Pt{110}(1 × 2) surface. The lowest-energy adsorption site for atomic H is the ridge bridge site (A), for which the calculated chemisorption energy and optimized H−Pt bond distance are 0.64 eV and 1.75 Å, respectively. Previous density functional theory calculations have similarly identified the ridge bridge site as the most stable site for hydrogen adatom adsorption on this surface.[87] The present calculations suggest that the potential energy surface is relatively flat in the region of the ridge sites, and the trough sites are comparatively less favorable energetically. The results suggest that hydrogen diffusion may take place preferentially along and across the close-packed ridge rows as opposed to across the troughs on the missing-row reconstructed surface.

Thermal desorption experiments have indicated that hydrogen adsorbs dissociatively on the Pt{110}(1 × 2) surface in two distinct states, designated β_1 and β_2.[88,89] A third α state has also been reported in the thermal desorption spectra, the appearance of which was thought to be sensitive to the quality of the crystal.[90] The β_2 adstate, which is associated with the higher desorption peak temperature, is populated at low coverages, followed by the β_1 state with increasing hydrogen exposure, and the two adstates have been interpreted in terms of adsorption in different sites on the surface. The adatom coverage of 0.25 ML investigated in the density functional theory calculations corresponds experimentally to the population of the β_2 state, for which the experimentally determined activation energy for desorption is 1.15 eV/H_2 or 0.57 eV/($^1/_2$)H_2 at this coverage.[88] The experimental activation energy for desorption is similar to the calculated chemisorption energies obtained in the present work for adsorption in the ridge sites (Table 5).

It should be noted that the activation energy for desorption at 0.25 ML determined in the detailed analysis of the thermal desorption spectra[88] may be equated with the differential heat of adsorption for nonactivated adsorption. In contrast, the chemisorption energies calculated in the present work for each site at an adatom coverage of 0.25 ML correspond to an estimate of the integral heat of adsorption, assuming that all adatoms occupy the same type of adsorption site. The experimentally determined activation energy for recombinant desorption from the β_2 state exhibits a strong dependence on the adatom coverage,[88] which has been attributed to the presence of both attractive next-nearest-neighbor and repulsive nearest-neighbor adsorbate−adsorbate interactions on the surface. The chemisorption energies (integral heat of adsorption) calculated at 0.25 ML for each site (Table 5) should therefore not be directly equated with the experimentally determined activation energy for desorption from the β_2 state at 0.25 ML.

The β_2 state has been associated with adsorption in the pseudo-4-fold sites in the trough on the basis of work function measurements,[88,89,91] photoemission of coadsorbed xenon studies,[92] and XPS measurements of core-level shifts,[93] and the lower-binding-energy β_1 state has been identified with adsorption on the {111} facets.[88,90] The results of the calculations summarized in Table 5, however, suggest that the trough sites are less stable than the ridge sites.

He-diffraction measurements by Kirsten et al.[94] have further revealed that adsorption in the β_2 state results in an increase in the corrugation amplitude of the Pt{110}(1 × 2) surface. Although the authors argue in favor of the population of subsurface sites below the ridge atoms with a concomitant expansion of the first interlayer spacing, they note that adsorption in the ridge bridge sites could equally well explain the observed increase in corrugation. To be consistent with the observed results, the authors proposed an adsorption geometry for hydrogen in the ridge bridge site with a H−Pt distance of 1.8 Å at a height of 1.1 Å above the ridge atoms, which is in surprisingly good agreement with the corresponding values of 1.75 and 1.03 Å calculated for this site in the present study. It should, however, be noted that the possibility of adsorption in subsurface sites cannot be negated on the basis of the results of the present calculations because such sites were not explicitly treated in this study.

F. Comparison of the Stable Intermediates. The most stable adsorption site determined for CH_x ($x = 1-3$) chemisorption on Pt{110}(1 × 2) is the site that not only completes the tetravalency of the carbon atom but also involves the maximum possible number of ridge substrate atoms for a site of that type. Methyl (CH_3) thus preferentially occupies the ridge atop site; methylene (CH_2), the ridge bridge site; and methylidyne (CH), the fcc 3-fold site involving two ridge atoms. The trend in the completion of the tetravalency of the carbon atom is further extended to carbon adatom adsorption on Pt{110}(1 × 2), with atomic carbon adsorption preferentially favoring the 4-fold pseudo-subsurface site in the trough at 0.25 ML.

The calculated chemisorption energy for each adsorbate in the lowest-energy site increases with the number of C−Pt bonds formed (i.e., with the increase in the valency of the CH_x fragment). The calculated chemisorption energy is 2.33 eV for CH_3, increasing to 4.61 eV for CH_2, 6.72 eV for CH, and 7.19 eV/C atom. The bonding analysis for each species reveals that in all cases the highest occupied molecular orbital plays the dominant role in the formation of the covalent adsorbate−substrate bond. Adsorption on the surface results in a net transfer of electrons to the adsorbate in all cases, the magnitude of which decreases with a decrease in the valency of the species. For CH, a net charge of $-0.20e$ accumulates on the adsorbate, decreasing to $-0.13e$ for methylene and $-0.10e$ for methyl as calculated within the Bader topological model.[70,71] This trend may be related to the increased population of the adsorbate valence orbitals, which are involved in the formation of the adsorbate−substrate bond, as the valency of the species decreases.

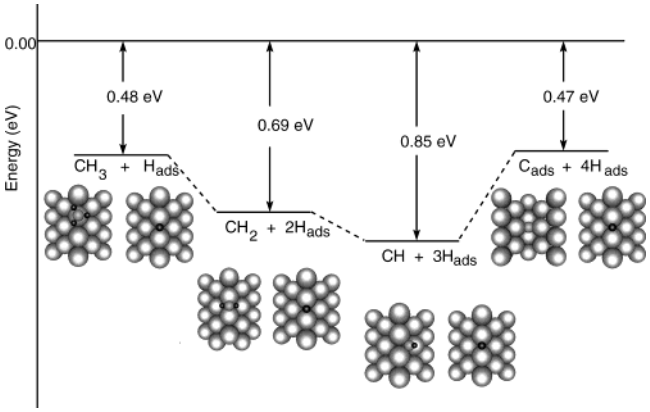

Figure 11. Electronic energy diagram of CH_x ($x = 0-3$) intermediates adsorbed in their most stable sites on Pt{110}(1 × 2). The energy zero corresponds to the clean Pt{110}(1 × 2) slab and an isolated methane molecule.

On the basis of the calculations for CH_x ($x = 0-3$) and atomic hydrogen chemisorption in the most stable sites on Pt{110}-(1 × 2), the electronic energy diagram shown in Figure 11 may be constructed, in which the energy is referenced to free methane and the clean Pt surface and hydrogen adatom coadsorption at infinite separation from the adsorbed radical is assumed. Methylidyne is found to be the most stable species on the Pt{110}(1 × 2) surface, in agreement with molecular beam experiments by Watson et al.[12,13] in which methylidyne was demonstrated to be the stable methane dissociation intermediate at all coverages in the surface-temperature range of 300−450 K. Methylidyne has similarly been found to be the most stable intermediate on Pt{111} using both periodic slab[62] and cluster calculations[33,58] as well as on a range of related transition metals.[58] It is worth emphasising that although the equilibrium distribution of CH_x fragments on the surface is governed by thermodynamic considerations their rate of accumulation on the surface is determined by the corresponding kinetic parameters. The determination of the activation energy barriers for each sequential CH_x dehydrogenation reaction thus forms the subject of the second part of this publication.

IV. Conclusions

CH_x ($x = 0-3$) chemisorption on Pt{110}(1 × 2) has been investigated using density functional theory periodic slab calculations. CH_3 preferentially occupies the ridge atop site; CH_2, the ridge bridge site; and CH, the fcc 3-fold site on the {111} microfacets of the missing-row reconstructed surface. The lowest-energy site for atomic carbon adsorption is a pseudo-subsurface 4-fold site at the bottom of the trough. With atomic hydrogen coadsorbed in the most stable ridge bridge site, CH is demonstrated to be the energetically most stable of the CH_x ($x = 0-3$) fragments adsorbed on Pt{110}(1 × 2).

Acknowledgment. We acknowledge financial support for this work from the EPSRC (U.K.) in the form of funds for workstations. M.A.P. thanks the Oppenheimer Trust for a research studentship and both the Cambridge Commonwealth

Trust and the ORS Awards Scheme for financial assistance. S.J.J. thanks the Royal Society for a University Research Fellowship.

References and Notes

(1) Zaera, F. *Chem. Rev.* **1995**, *95*, 2651.
(2) Bent, B. E. *Chem. Rev.* **1996**, *96*, 1361.
(3) Davis, S. M.; Somorjai, G. A. In *The Chemical Physics of Solid Surfaces and Heterogeneous Catalysis*; King, D. A., Woodruff, D. P., Eds.; Elsevier: Amsterdam, 1982; Vol. 4, p 217.
(4) Schulz, H. *Appl. Catal. A: General* **1999**, *186*, 3.
(5) Herrmann, W. A. *Angew. Chem., Int. Ed. Engl.* **1982**, *21*, 117.
(6) Röper, M. In *Catalysis in C1 Chemistry*; Keim, W., Ed.; Riedel: Dordrecht, The Netherlands, 1983.
(7) Biloen, P.; Sachtler, W. M. H. *Adv. Catal.* **1981**, *30*, 165.
(8) Van Hook, J. P. *Catal. Rev.—Sci. Eng.* **1980**, *21*, 1.
(9) Anderson, J. R., Boudert, M., Eds.; *Catalysis: Science and Technology*; Springer: Berlin, 1984; Vol. 5, p 1.
(10) Besenbacher, F.; Chorkendoff, I.; Clausen, B. S.; Hammer, B.; Molenbroek, A. M.; Nørskov, J. K.; Stensgaard, I. *Science* **1998**, *279*, 1913.
(11) Pitchai, R.; Klier, K. *Catal. Rev.—Sci. Eng.* **1986**, *28*, 13.
(12) Watson, D. T. P. Ph.D. Thesis, University of Cambridge, Cambridge, United Kingdom, 2001.
(13) Watson, D. T. P.; Titmuss, S.; King, D. A. *Surf. Sci.* **2002**, *505*, 49.
(14) Watson, D. T. P.; van Dijk, J.; Harris, J. J. W.; King, D. A. *Surf. Sci.* **2002**, *506*, 243.
(15) Walker, A. V.; King, D. A. *Phys. Rev. Lett.* **1999**, *82*, 5156.
(16) Walker, A. V.; King, D. A. *J. Chem. Phys.* **2000**, *112*, 4739.
(17) Walker, A. V.; King, D. A. *J. Chem. Phys.* **2000**, *112*, 1937.
(18) Walker, A. V.; King, D. A. *J. Phys. Chem. B* **2000**, *104*, 6462.
(19) Walker, A. V.; King, D. A. *Surf. Sci.* **2000**, *444*, 1.
(20) Watson, D. T. P.; Harris, J. J. W.; King, D. A. *J. Phys. Chem. B* **2002**, *106*, 3416.
(21) Watson, D. T. P.; Harris, J. J. W.; King, D. A. *Surf. Sci.* **2002**, *505*, 58.
(22) Petersen, M. A.; Watson, D. T. P.; Jenkins, S. J.; King, D. A. *J. Chem. Phys.* **2002**, *117*, 3951.
(23) Watson, D. T. P.; Ge, Q.; King, D. A. *J. Chem. Phys.* **2001**, *115*, 11306.
(24) Henderson, M. A.; Mitchell, G. E.; White, J. M. *Surf. Sci.* **1987**, *184*, L325.
(25) Zaera, F. *Langmuir* **1991**, *7*, 1998.
(26) Zaera, F.; Hoffmann, H. *J. Phys. Chem.* **1991**, *95*, 6297.
(27) Zaera, F. *Surf. Sci.* **1992**, *262*, 335.
(28) Liu, Z.-M.; Akhter, S.; Roop, B.; White, J. M. *J. Am. Chem. Soc.* **1988**, *110*, 8708.
(29) Ukraintsev, V. A.; Harrison, I. *Surf. Sci. Lett.* **1993**, *286*, L571.
(30) Fairbrother, D. H.; Peng, X. D.; Viswanathan, R.; Stair, P. C.; Trenary, M.; Fan, J. *Surf. Sci. Lett.* **1993**, *285*, L455.
(31) Fairbrother, D. H.; Peng, X. D.; Trenary, M.; Stair, P. C. *J. Chem. Soc., Faraday Trans.* **1995**, *91*, 3619.
(32) Oakes, D. J.; McCoustra, M. R. S.; Chesters, M. A. *Faraday Discuss.* **1993**, *96*, 325.
(33) Kua, J.; Goddard, W. A., III. *J. Phys. Chem. B* **1998**, *102*, 9492. Kua, J.; Goddard, W. A., III. *J. Phys. Chem. B* **1999**, *103*, 2318.
(34) Papoian, G.; Nørskov, J. K.; Hoffmann, R. *J. Am. Chem. Soc.* **2000**, *122*, 4129.
(35) Watwe, R. M.; Spiewak, B. E.; Cortright, R. D.; Dumesic, J. A. *J. Catal.* **1998**, *180*, 184.
(36) Minot, C.; van Hove, M. A.; Somorjai, G. A. *Surf. Sci.* **1982**, *127*, 441.
(37) Michaelides, A.; Hu, P. In *Theoretical Aspects of Heteogeneous Catalysis*; Nascimento, M. A. C., Ed.; Kluwer: Dordrecht, The Netherlands, 2001.
(38) Klinke, D. J., II; Wilke, S.; Broadbelt, L. J. *J. Catal.* **1998**, *178*, 540.
(39) Klinke, D. J., II; Dooling, D. J.; Broadbelt, L. J. *Surf. Sci.* **1999**, *425*, 334.
(40) Schüle, J.; Siegbahn, P.; Wahlgren, U. *J. Chem. Phys.* **1988**, *89*, 6982.
(41) Siegbahn, P. E. M.; Panas, I. *Surf. Sci.* **1990**, *240*, 37.
(42) Yang, H.; Whitten, J. L. *J. Am. Chem. Soc.* **1991**, *113*, 6442.
(43) Yang, H.; Whitten, J. L. *Surf. Sci.* **1991**, *255*, 193.
(44) De Koster, A.; van Santen, R. A. *J. Catal.* **1991**, *127*, 141.
(45) Burghgraef, H.; Jansen, A. P. J.; van Santen, R. A. *Surf. Sci.* **1995**, *324*, 345.
(46) Watwe, R. M.; Bengaard, H. S.; Rostrup-Nielsen, J. R.; Dumesic, J. A.; Nørskov, J. K. *J. Catal.* **2000**, *189*, 16.
(47) Michaelides, A.; Hu, P. *Surf. Sci.* **1999**, *437*, 362.
(48) Michaelides, A.; Hu, P. *J. Chem. Phys.* **2000**, *112*, 6006.
(49) Ciobîcă, I. M.; Frechard, F.; van Santen, R. A.; Kleyn, A. W.; Hafner, J. *Chem. Phys. Lett.* **1999**, *311*, 185.
(50) Ciobîcă, I. M.; Frechard, F.; van Santen, R. A.; Kleyn, A. W.; Hafner, J. *J. Phys. Chem. B* **2000**, *104*, 3364.
(51) Ciobîcă, I. M.; van Santen, R. A. *J. Phys. Chem. B* **2002**, *106*, 6200.
(52) Paul, J.-F.; Sautet, P. *J. Phys. Chem. B* **1998**, *102*, 1578.
(53) Bertani, V.; Cavallotti, C.; Masi M.; Carrà, S. *J. Phys. Chem. A* **2000**, *104*, 11390.
(54) Zhang, C. J.; Hu, P. *J. Chem. Phys.* **2002**, *116*, 322.
(55) Zheng, C.; Apeloig, Y.; Hoffmann, R. *J. Am. Chem. Soc.* **1988**, *110*, 749.
(56) Au, C.-T.; Liao, M.-S.; Ng, C.-F. *J. Phys. Chem. A* **1998**, *102*, 3959.
(57) Au, C.-T.; Ng, C.-F.; Liao, M.-S. *J. Catal.* **1999**, *185*, 12.
(58) Kua, J.; Faglioni, F.; Goddard, W. A., III. *J. Am. Chem. Soc.* **2000**, *122*, 2309.
(59) Ge, Q.; Neurock, M.; Wright, H. A.; Srinivasan, N. *J. Phys. Chem. B* **2002**, *106*, 2826.
(60) Michaelides, A.; Hu, P. *J. Chem. Phys.* **2001**, *114*, 2523.
(61) Yang, Q. Y.; Maynard, K. J.; Johnson, A. D.; Ceyer, S. T. *J. Chem. Phys.* **1995**, *102*, 7734.
(62) Michaelides, A.; Hu, P. *J. Am. Chem. Soc.* **2000**, *122*, 9866.
(63) *CASTEP 3.9* and *4.2* academic versions, licensed under the UKCP-MSI Agreement, 1999. Payne, M. C.; Teter, M. P.; Allan, D. C.; Arias, T. A.; Joannopoulos, J. D. *Rev. Mod. Phys.* **1992**, *64*, 1045.
(64) Perdew, J. P.; Chevary, J. A.; Vosko, S. H.; Jackson, K. A.; Pederson, M. R.; Singh, D. J.; Fiolhais, C. *Phys. Rev. B* **1992**, *46*, 6671.
(65) Vanderbilt, D. *Phys. Rev. B* **1990**, *41*, 7892.
(66) Lide, D. R., Ed.; *Handbook of Chemistry and Physics*, 75th ed.; CRC Press LCC: New York, 1998.
(67) Monkhorst, H. J.; Pack, J. D. *Phys. Rev. B* **1976**, *13*, 5188.
(68) Gillan, M. J. *J. Phys.: Condens. Matter* **1989**, *1*, 689.
(69) De Vita, A.; Gillan, M. *J. Phys.: Condens. Matter* **1991**, *3*, 6225.
(70) Bader, R. F. W. *Atoms in Molecules: A Quantum Theory*; Oxford University Press: Oxford, England, 1990.
(71) Popelier, P. *Atoms in Molecules: An Introduction*; Pearson Education: Harlow, UK, 2000.
(72) Yamagishi, S.; Jenkins, S. J.; King, D. A. *Chem. Phys. Lett.* **2003**, *367*, 116.
(73) Yamagishi, S.; Jenkins, S. J.; King, D. A. *J. Chem. Phys.* **2002**, *117*, 819.
(74) Yamagishi, S.; Jenkins, S. J.; King, D. A. *J. Chem. Phys.* **2001**, *114*, 5765.
(75) Held, G.; Braun, W.; Steinrück, H.-P.; Yamagishi, S.; Jenkins, S. J.; King, D. A. *Phys. Rev. Lett.* **2001**, *87*, 216102.
(76) Jenkins, S. J.; Ge, Q.; King, D. A. *Phys. Rev. B* **2001**, *64*, 012413.
(77) Ge, Q.; Jenkins, S. J.; King, D. A. *Chem. Phys. Lett.* **2000**, *327*, 125.
(78) Kellogg, G. L. *Phys. Rev. Lett.* **1985**, *55*, 2168.
(79) Fery, P.; Moritz, W.; Wolf, D. *Phys. Rev. B* **1988**, *38*, 7275.
(80) Sowa, E. C.; van Hove, M. A.; Adams, D. L. *Surf. Sci.* **1988**, *199*, 174.
(81) Jenkins, S. J.; Petersen, M. A.; King, D. A. *Surf. Sci.* **2001**, *494*, 159.
(82) The term agostic was coined by Brookhart and Green,[83] who used it in the context of organometallic compounds. An agostic interaction refers to situations in which a hydrogen atom is covalently bonded simultaneously to both a carbon atom and a transition-metal atom.
(83) Brookhart, M.; Green, M. L. H. *J. Organomet. Chem.* **1983**, *250*, 395.
(84) Goddard, W. A. *Science* **1985**, *227*, 917.
(85) Goddard, W. A. *Science* **1985**, *228*, 130.
(86) Stuck, A.; Wartnaby, C. E.; Yeo, Y. Y.; King, D. A. *Phys. Rev. Lett.* **1995**, *578*, 74.
(87) Horch, S.; Lorensen, H. T.; Helveg, S.; Lægsgaard, E.; Stensgaard, I.; Jacobsen, K. W.; Nørskov, J. K.; Besenbacher, F. *Nature* **1999**, *398*, 134.
(88) Engstrom, J. R.; Tsai, W.; Weinberg, W. H. *J. Chem. Phys.* **1987**, *87*, 3104.
(89) Shern, C. S. *Surf. Sci.* **1992**, *264*, 171.
(90) Anger, G.; Berger, H. F.; Luger, M.; Feistritzer, S.; Winkler, A.; Rendulic, K. D. *Surf. Sci.* **1989**, *219*, L583.
(91) Shern, C. S. *Chin. J. Phys.* **1992**, *30*, 841.
(92) Ducros, R.; Fusy, J. *Surf. Sci.* **1988**, *207*, L943.
(93) Dückers, K.; Prince, K. C.; Bonzel, H. P.; Cháb, V.; Horn, K. *Phys. Rev. B* **1987**, *36*, 6292.
(94) Kirsten, E.; Parschau, G.; Stocker, W.; Rieder, K. H. *Surf. Sci. Lett.* **1990**, *231*, L183.